

# Jet momentum reconstruction in the QGP background with machine learning

Ran Li,<sup>1</sup> Yi-Lun Du,<sup>2,\*</sup> and Shanshan Cao<sup>1,†</sup>

<sup>1</sup>*Institute of Frontier and Interdisciplinary Science, Shandong University, Qingdao, 266237, China*

<sup>2</sup>*Shandong Institute of Advanced Technology, Jinan 250100, China*

(Dated: December 10, 2024)

We apply a Dense Neural Network (DNN) approach to reconstruct jet momentum within a quark-gluon plasma (QGP) background, using simulated data from PYTHIA and Linear Boltzmann Transport (LBT) Models for comparative analysis. We find that medium response particles from the LBT simulation, scattered out of the QGP background but belonging to medium-modified jets, can inevitably lead to oversubtraction of the background if the DNN model is trained on vacuum jets from PYTHIA simulation. By training the DNN model on quenched jets generated using the LBT model, we significantly reduce this prediction bias and achieve more accurate background subtraction compared to conventional Area-based and Constituent Subtraction methods widely adopted in experimental measurements. Additionally, we develop a matching procedure to pair reconstructed jets inside a background to their counterparts reconstructed without the background, further improving the reliability of ML models in background subtraction, and therefore enabling an accurate capture of the jet quenching effect and a precise estimation of the nuclear modification factor of jets in high-energy nuclear collisions.

## I. INTRODUCTION

Jets, collimated sprays of particles originating from splittings and hadronization of energetic partons produced in hard collisions between nucleons, serves as an excellent probe of the quark-gluon plasma (QGP) created in relativistic heavy-ion collisions [1–4]. Scatterings between jet partons and the QGP can result in significant suppression, or “quenching”, of the jet spectra in nucleus-nucleus (A+A) collisions relative to their baselines in proton-proton ( $p + p$ ) collisions [5]. The jet transport coefficient inside the QGP extracted from the jet quenching data appears an order of magnitude larger than that inside a cold nucleus probed by deeply inelastic scatterings [6–9], revealing the partonic degrees of freedom inside the QGP. Considerable efforts have been dedicated into understanding the interaction dynamics between jets and the QGP [10–16] and developing sophisticated Monte-Carlo event generators to simulate jet scatterings through the QGP [17–25]. These enable us to extend studies on jets from the quenching of their yields to nuclear modification of their substructures [26–38], and from improving model descriptions of the jet data to quantitatively extracting various QGP properties using the jet data [39–41].

While it is straightforward to track jet particles from their initial production to their subsequent splittings and hadronization in theoretical simulations, it is a great challenge to identify jet particles in relativistic nuclear collision experiments due to the background of particles produced from multi-parton interactions in the initial state or the QGP medium in the final state. Proper ways of subtracting these backgrounds in experiments are es-

sential for correctly extracting jet observables for a meaningful comparison to theoretical predictions. Therefore, tremendous dedication has been devoted in designing efficient background subtraction methods. For instance, for jet momentum reconstruction, conventional schemes such as the Area-based method [42, 43] and the Constituent Subtraction method [44, 45] have been developed. They rely on estimating and subtracting the average background contributions after excluding the leading jets, however, tend to discard subtle features of individual jets, and thus often result in large residual fluctuations. While being effective in  $p + p$  collisions, these methods may struggle in heavy-ion collisions due to the complicated interactions between jets and the QGP. In the presence of the QGP, subtraction can be biased by recoil particles from the medium and other noise sources, leading to inaccurate reconstruction of jet momentum and substructures, especially for jets with low transverse momenta ( $p_T$ ). This highlights the necessity for establishing more flexible and accurate approaches that can adapt to complex backgrounds, and capture rich features of individual quenched jets in heavy-ion collisions.

Recent advancements in machine learning (ML) have shown significant promise in heavy-ion physics [39, 46–66], particularly in the study of jet quenching in QGP [67]. Specifically, ML techniques have been successfully applied to the classification between quark and gluon jets [68, 69], identification of quenched jets [70–74], prediction of jet energy loss [75, 76] and locating jet creation vertices [77], demonstrating their potential to capture subtle features of jet modifications in a QGP environment. Regarding to background subtraction, ML also offers a powerful approach to extract the momenta of jets embedded in QGP backgrounds by learning patterns of jet signals inside backgrounds on a jet-by-jet basis [78–80]. In Ref. [78], jets from PYTHIA simulation [81, 82] are placed in a thermal background for model training, suggesting that the ML-based reconstruction approach

\* yilun.du@iat.cn

† shanshan.cao@sdu.edu.cn

achieves superior precision in jet momentum reconstruction compared to the conventional Area-based method. This ML-based method has been further applied to the ALICE experimental data where the nuclear modification factor ( $R_{AA}$ ) has been obtained for jets with  $p_T$  down to 30 to 40 GeV [79]. Considering that PYTHIA simulates jet production in  $p+p$  collisions, different medium modification effects in A+A collisions, such as the variation of the quark-to-gluon-jet fraction, medium-induced gluon emission, and jet-induced medium excitation, are incorporated separately in modifying the training data, based on which the systematic error of  $R_{AA}$  from implementing different ML models is estimated in Ref. [79].

For an improved treatment of medium modification of jets, in this work, we will adopt the state-of-the-art Linear Boltzmann Transport (LBT) model [24] to generate data of quenched jets for training neural networks, and compare its performance to that of both conventional methods and ML models trained with the PYTHIA data. We will not only focus on evaluating the precision of the ML-based jet reconstruction method on predicting the jet momentum, but also develop a matching procedure for further enhancing the ability to identify real jets, or exclude fake jets, in analyzing jet observables. The remainder of this paper is structured as follows. In Sec. II, we introduce the models for simulating jets and thermal backgrounds in high-energy nuclear collisions. Section III discusses different background subtraction methods, including the Area-based method, the Constituent Subtraction method, and the ML method. The matching procedure we design for eliminating fake jet contribution is also introduced. In Sec. IV, we present results on the jet momentum reconstruction and the jet  $R_{AA}$ , and compare them between different background subtraction methods. Finally, we summarize in Sec. V.

## II. SIMULATION MODELS

We train neural networks using simulation models that capture the essential features of jet formation and their interactions with the QGP. Below, we briefly introduce the three key models employed in this work: the PYTHIA model of jet production in  $p+p$  collisions, the LBT model for jet-QGP interactions, and a toy thermal model for mimicking the QGP background.

PYTHIA [81, 82] is a widely-used event generator for simulating high-energy particle collisions, such as those conducted at the Large Hadron Collider (LHC). It can model the formation of jets in quantum chromodynamics (QCD) processes that start with hard scatterings between partons from projectile and target nucleons. Highly virtual partons produced from these hard scatterings then evolve to lower scales by sequential splittings. This is known as parton shower. As the daughter partons from these splittings approach the hadronization scale, they are converted into hadrons based on the Lund string model. One may further apply jet finding algorithms,

such as the anti- $k_T$  [83] and Cambridge–Aachen [84, 85] algorithms to cluster these hadrons into jets and compare their observables to experimental data. In the context of studying nuclear modification of jets in heavy-ion collisions, PYTHIA provides a baseline of  $p+p$  collisions that excludes jet quenching effects.

The Linear Boltzmann Transport (LBT) model [24, 86] simulates elastic and inelastic scatterings between jet partons and thermal partons inside the QGP based on the Boltzmann equation. The elastic scattering rates of jet partons are calculated using the leading-order matrix elements of  $2 \rightarrow 2$  processes, with all possible partonic scattering channels taken into account [87]; and the inelastic scattering rates are related to the spectra of medium-induced gluon emissions from jet partons, which can be evaluated using the higher-twist energy loss formalism [88–96]. The LBT model keeps track of not only the initially produced jet partons and their emitted gluons inside the QGP, but also the medium partons that are scattered out of the thermal background (named as “recoil” partons) and the energy holes left behind (named as “negative” partons). These recoil and negative partons constitute medium response to jet propagation in LBT, which is naturally included in medium-modified jets and has been shown to be essential to jet observables related to soft particles at large angles relative to jet axes. The initially produced jet partons, their emitted gluons, recoil partons and negative partons all belong to “jet partons” produced by the LBT model. Contributions from negative partons are subtracted from those of other jet partons for all jet observables. By combining the LBT model with a QGP background simulated by the (3+1)-dimensional viscous hydrodynamic model CLVisc [97, 98], one can achieve good descriptions of the quenching of hadrons and jets [99, 100], their collective flows [101], and jet substructures [33]. In the present work, we use the LBT model to further evolve partons produced by PYTHIA inside the QGP. Its output data allow ML models to learn the complex energy dissipation patterns and structural changes in jets due to their interactions with the QGP. Consequently, the LBT model provides a valuable tool for developing and validating ML approaches that aim to accurately reconstruct jet observables in relativistic heavy-ion experiments.

To study the ML techniques in reconstructing jet momentum in the presence of a QGP background, we embed jet partons produced by either PYTHIA or PYTHIA+LBT into a background generated by a thermal toy model [45]. For each jet event, the thermal model is tuned to produce  $\pi^\pm$  particles whose momenta follow a Boltzmann distribution with a total multiplicity of 1538 and an average transverse momentum  $\langle p_T \rangle = 0.5696$  GeV within the rapidity range of  $|y| < 1$ , mimicking the realistic soft hadron environment created in central (0-10%) Pb+Pb collisions at  $\sqrt{s_{NN}} = 5.02$  TeV [102]. In principle, one can also sample background particles from the freezeout hypersurface of the same hydrodynamic medium used for simulating jet-QGP interactions. How-

ever, for the purpose of comparing to earlier studies on this topic [78, 79], we keep using a thermal toy model for generating the background, which should also be sufficient for a proof-of-principle study on applying ML techniques to jet reconstruction at this moment.

In this work, we generate 360k parton-level jets using PYTHIA 8 with the Monash 2013 tune [103]. The same set of PYTHIA jets are then evolved using the LBT model coupled to a QGP medium for central (0–10%) Pb+Pb collisions at  $\sqrt{s_{\text{NN}}} = 5.02$  TeV. The production vertices of jets in heavy-ion collisions are sampled using the Monte-Carlo Glauber model. Each jet parton is assumed to stream freely before its formation time and the thermalization time of the QGP (0.6 fm). The formation time of a jet parton is evaluated by summing over the splitting times of its ancestors in PYTHIA vacuum showers [104]. After that, jet partons interact with the QGP within LBT until the local temperature of the medium drops below the hadronization temperature (165 MeV). The strong coupling constant in LBT is set as  $\alpha_s = 0.15$ . After jet-medium interactions, 260k medium-modified jets are obtained. Jet reconstruction is performed using the anti- $k_T$  algorithm with a radius parameter of  $R = 0.4$  for both PYTHIA and PYTHIA+LBT jets, either with or without the thermal background contributions. For analysis, we select jets within the transverse momentum range of  $5 \text{ GeV} < p_T < 160 \text{ GeV}$  and pseudorapidity range of  $|\eta| < 1 - R$ . For the rest of this work, we will use the notation “LBT” to abbreviate “PYTHIA+LBT” in describing how we generate the jet data. On the other hand, the notation “PYTHIA+LBT” will be saved for describing the combination of jet data generated by PYTHIA simulation and (PYTHIA+)LBT simulation in training ML models.

### III. BACKGROUND SUBTRACTION METHODS

Two conventional background subtraction methods and a ML method will be used for a comparative study. We also adopt a jet matching procedure to identify the original PYTHIA or LBT jet in the absence of background particles associated with a reconstructed jet embedded in a background.

#### A. Area-based Method

The Area-based method [42, 43] is a widely adopted approach for jet momentum reconstruction, which is effective in mitigating impact of the background noise, such as contributions from underlying events in high-energy collisions. It first estimates the density of the background as the median value of transverse momentum densities of clusters reconstructed using the  $k_T$  algorithm [105, 106], with a few (two in this work) hardest clusters excluded:

$$\rho = \text{median}(p_{T,i}/A_i), \quad (1)$$

where  $p_{T,i}$  is the  $p_T$  of the  $i$ -th cluster, and  $A_i$  is its area given by the ghost particle method. With this background density, the  $p_T$  of an anti- $k_T$  jet is then given by

$$p_{T,\text{jet}}^{\text{Area-based}} = p_{T,\text{jet}}^{\text{within bkg}} - \rho A, \quad (2)$$

where the first part on the right denotes the  $p_T$  of a jet reconstructed using the anti- $k_T$  algorithm in the presence of the background, and  $A$  denotes the area of this jet.

#### B. Constituent Subtraction Method

Unlike the Area-based method which subtracts a smooth background from a jet, the Constituent Subtraction method [44, 45] is designed to reduce the background noise by adjusting momenta of individual particles or removing individual particles within an event. This method is particularly useful in high-background environments, such as heavy-ion collisions, where the large number of soft background particles can introduce clustering biases [107]. To reduce these biases, the Constituent Subtraction method subtracts the background at the particle level before performing jet clustering, thereby minimizing its impact on finding “correct” jets.

The Constituent Subtraction method starts with estimating the average background density  $\rho$  of an event in the same way as discussed earlier for the Area-based method. Then, to emulate the background particle distribution, a large number of soft ghost particles are introduced, which uniformly cover the rapidity-azimuthal-angle  $(y, \phi)$  plane under investigation. Each ghost particle here is assigned a transverse momentum of  $p_T^g = \rho A^g$ , where  $A^g$  is the area of a ghost particle. The total transverse momentum of ghost particles approximates that of the background.

For each pair of (real) particle  $i$  and ghost  $k$ , their distance is defined as

$$\Delta R_{i,k} = p_{T,i}^\alpha \sqrt{(y_i - y_k^g)^2 + (\phi_i - \phi_k^g)^2}, \quad (3)$$

where  $\alpha$  is a free parameter, set to 1 here. This distance incorporates a weight of the particle  $p_T$ , considering that background particles generally have lower  $p_T$  than particles initiated by hard scatterings. By sorting these distances in an ascending order, the momentum removal begins with the smallest distance. For each pair, the transverse momenta of particle  $i$  and ghost  $k$  are adjusted as follows:

$$\begin{aligned} p_{T,i} &\rightarrow p_{T,i} - p_{T,k}^g, & p_{T,k}^g &\rightarrow 0, & \text{if } p_{T,i} &\geq p_{T,k}^g; \\ p_{T,k}^g &\rightarrow p_{T,k}^g - p_{T,i}, & p_{T,i} &\rightarrow 0, & \text{otherwise.} \end{aligned}$$

The removal process stops when  $\Delta R_{i,k} > \Delta R^{\text{max}}$  where  $\Delta R^{\text{max}}$  is a free parameter controlling the maximum range of neighboring ghosts considered for subtraction. We set  $\Delta R^{\text{max}}$  as  $\infty$ . After these momentum subtractions, jets are reconstructed from particles with nonzero

momenta using the anti- $k_T$  algorithm, allowing for a straightforward determination of their  $p_T$ .

By locally adjusting the momentum of each particle based on the background density, this Constituent Subtraction method is expected to isolate the jet signal while preserving the overall jet momentum and substructure. This feature is crucial for analyzing jet properties in high-background environments.

### C. Machine Learning Method

Dense neural networks (DNNs) are powerful tools for mapping input observations to output targets. Unlike conventional methods, neural networks do not require explicit mathematical models or intricate pre-computations. Instead, they autonomously extract features and establish mapping rules by learning from large datasets. This makes them particularly well-suited for problems involving high-dimensional and complex data structures.

In this work, we leverage neural networks to predict the jet momentum, following the approach in Ref. [78]. The input jet observables used in the model include:

- Uncorrected jet momentum reconstructed by the jet finding algorithm;
- Jet transverse momentum, corrected by the Area-based method;
- Jet substructure observables: mass, angularity, momentum dispersion, and the difference between the momenta of the leading and sub-leading constituent tracks (LeSub);
- Number of constituents within the jet;
- Mean and median transverse momenta of all constituents;
- Transverse momenta of the first ten hardest particles within the jet.

The target value of the jet momentum after the background subtraction,  $p_{T,\text{jet}}^{\text{target}}$ , is defined as the  $p_T$  sum of the raw jet particles generated by the PYTHIA or LBT simulation within the jet reconstructed in the presence of the QGP background:

$$p_{T,\text{jet}}^{\text{target}} = \sum_{i \in \text{PYTHIA/LBT}} p_{T,i}, \quad (4)$$

where  $i$  labels constituents within the reconstructed jet. Therefore, this  $p_{T,\text{jet}}^{\text{target}}$  represents the  $p_T$  contributed by the “true” jet partons originating from the PYTHIA or LBT model, excluding contributions from the background particles.

The DNN architecture employed in this study consists of three hidden layers containing 100, 100, and 50 nodes, respectively. Each neuron uses the Rectified Linear Unit (ReLU) activation function, defined as

$\text{ReLU}(x) = \max(x, 0)$ , to introduce non-linearity and efficiently model complex relationships in the data. The loss function chosen for training is the LogCosh function,  $\log[\cosh(x)]$ , which behaves as  $x^2/2$  for small  $x$  and  $\text{abs}(x) - \log(2)$  for large  $x$ . This property makes it robust to outliers while maintaining smooth sensitivity to small residuals. The Adam optimization algorithm [108] is employed to minimize the loss function during training, offering adaptive learning rates for efficient convergence. The dataset is split into training and testing subsets, with 80% of the simulated jet data used for training the DNN model and the remaining 20% reserved for testing its performance. This division ensures the model’s ability to generalize its predictions to unseen data while preventing overfitting.

### D. Jet Matching

As discussed in Sec. III B, a strong medium background can introduce clustering bias. In other words, jet partons which should be clustered into one jet in the absence of the QGP background may no longer belong to the same jet when the background particles also participate in jet clustering. Therefore, even the Area-based method or the ML method can cleanly remove the background components within a jet reconstructed inside a background, it still cannot accurately reproduce properties of jets that have never been contaminated by background. Meanwhile, background fluctuations may lead to “fake” jets, which have no connection to real jets originating from the initial nucleon-nucleon hard scatterings. All the three background subtraction methods discussed above would suffer from these fake jets especially for low  $p_T$  jets.

To estimate the error introduced by such jet mismatching, and further improve the ML performance on predicting the  $p_T$  of “real” jets, we employ the following jet matching procedure. For each jet reconstructed inside a background  $j_{\text{in bkg}}$ , we search for its counterpart  $j_{\text{real}}$  from its corresponding PYTHIA or LBT event in the absence of the background. We require the distance between  $j_{\text{in bkg}}$  and  $j_{\text{real}}$  satisfy  $\Delta R = \sqrt{\Delta\eta^2 + \Delta\phi^2} < 0.4$ . If multiple jets from the PYTHIA or LBT event satisfy this condition, the one with the smallest  $R$  is identified as  $j_{\text{real}}$  for  $j_{\text{in bkg}}$ . On the other hand, if no  $j_{\text{real}}$  can be found,  $j_{\text{in bkg}}$  is identified as a fake jet. The ML method discussed in Sec. III C can then be updated by replacing its target value from Eq. (4) to the  $p_T$  of  $j_{\text{in bkg}}$ . Details of this update will be discussed later in Sec. IV B when this matching procedure is applied.

## IV. RESULTS

### A. Jet Momentum Reconstruction

Following Ref. [78], we first train the ML model on the PYTHIA data and evaluate its performance on three

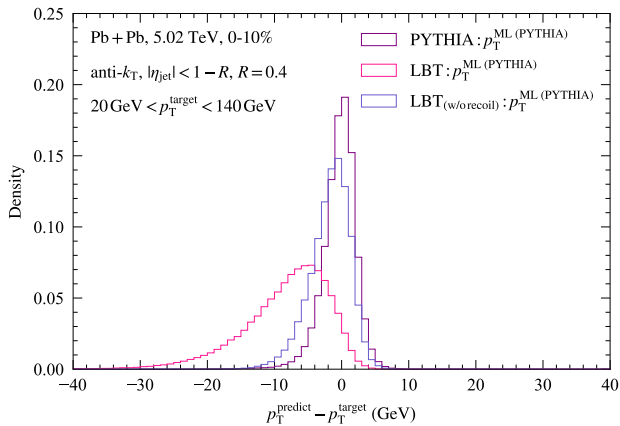


FIG. 1. (Color online) Residual distributions of the jet  $p_T$  predicted by the ML model trained on the PYTHIA data, compared between testing on datasets of PYTHIA, LBT, and LBT without recoil (and negative) particles, respectively.

datasets from three different model setups: PYTHIA, LBT, and LBT without medium response particles. In the last setup, we implement the same LBT simulation as described in Sec. II, except that we do not include recoil and negative particles in our test dataset. Here, offsprings of recoil particles are also labeled as “recoil” and excluded in the last setup. If not otherwise specified, background particles from the thermal model are included in both training and testing data. Figure 1 presents the corresponding residual distributions of the jet  $p_T$ , i.e., distributions of  $\delta p_T = p_T^{\text{predict}} - p_T^{\text{target}}$ , with  $p_T^{\text{predict}}$  the value predicted by our ML model for a jet embedded in a background, and  $p_T^{\text{target}}$  its corresponding target value as defined in Eq. (4). Here, tests are conducted on jets with a cone size of  $R = 0.4$  and target  $p_T$  within (20, 140) GeV. The results in Fig. 1 demonstrate the ML model trained by the PYTHIA data can accurately predict the  $p_T$  of the PYTHIA jets, with a mean residual close to zero and a narrow width of the distribution. However, for its prediction on the LBT jets, a notable negative bias emerges for the ML model trained by the PYTHIA data, suggesting an underestimation of the jet  $p_T$  due to an oversubtraction of the QGP background. This results from different inner structures between vacuum (PYTHIA) jets and medium-modified (LBT) jets. The latter contains a large number of soft medium-response particles that originate from the QGP background. These particles have similar features to the background particles but should belong to medium-modified jets. Therefore, if the ML model is trained using the PYTHIA data, which do not include these medium response components, these components are very likely to be identified as background particles and subtracted from the LBT jets by mistake. To verify this cause, we further test the ML model on the LBT data with medium response (recoil and negative) particles removed. This removal significantly improve the accuracy of the ML

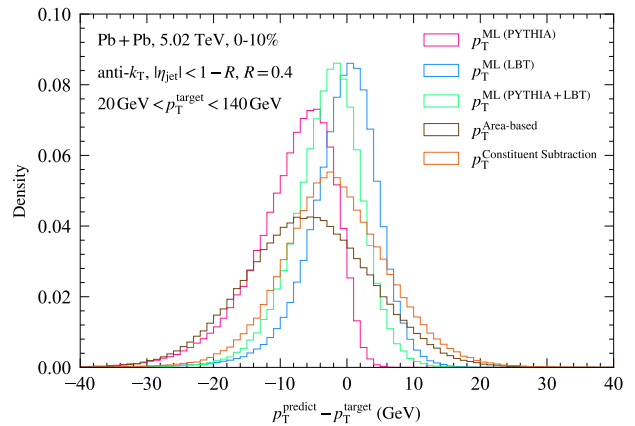


FIG. 2. (Color online) Residual distributions of the jet  $p_T$  predicted by different estimators, ML models trained on the PYTHIA, LBT, and combined PYTHIA+LBT data, and the conventional Area-based and Constituent Subtraction methods. The testing dataset is generated by the LBT model.

Estimator	Testing Data	Fitting (GeV)	
		Mean	$\sigma$
ML(PYTHIA)	PYTHIA	-0.5	2.0
ML(PYTHIA)	LBT	-7.1	5.3
ML(PYTHIA)	LBT(w/o recoil)	-1.7	2.7
ML(LBT)	LBT	-0.4	4.5
ML(PYTHIA+LBT)	LBT	-2.9	4.6
Area-based	LBT	-6.3	9.4
Constituent Subtract.	LBT	-2.5	7.4

TABLE I. The means and standard deviations of the residual distributions of the jet  $p_T$  from different estimators evaluated on different testing datasets.

model prediction. The comparison shown in Fig. 1 underscores the importance of training the ML model using jet data that include jet-medium interaction effects to ensure accurate background subtraction in heavy-ion collisions.

In Fig. 2, we compare the predictions on the jet  $p_T$  from different ML models and conventional background subtraction methods. Three different ML models are applied, trained using the PYTHIA, LBT, and combined PYTHIA+LBT data, respectively. All models are tested against the LBT data embedded in a thermal background. Again, we see a negative bias in the residual distribution of the jet  $p_T$  using the ML model trained on the PYTHIA data due to its incapability of recognizing the medium response particles. By training the ML model using the combined dataset from the PYTHIA and LBT simulations, this bias can be significantly reduced. The ML model trained solely on the LBT data presents the best performance, with a mean value of the distribution closest to zero and a narrowest width. The two conventional methods, the Area-based and Constituent Subtraction methods, also show oversubtractions of the background due to overestimations of the background density

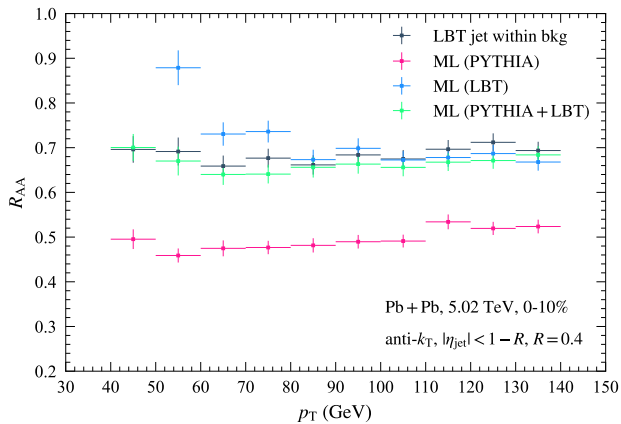


FIG. 3. (Color online) The nuclear modification factor of jets obtained from ML models trained on the PYTHIA, LBT, and combined PYTHIA+LBT datasets, compared to a baseline of the LBT jets reconstructed in the presence of a QGP background (LBT jet within bkg).

resulting from the contribution of recoil particles outside jet cones. The widths of the residual distributions from these two conventional methods are apparently larger than those from the LBT-trained and PYTHIA+LBT-trained ML models. Note that while Eq. (4) can also be applied to evaluate  $p_T^{\text{target}}$  in the Area-based method, it cannot be applied to the Constituent Subtraction method in which jets are constructed after background subtraction. For each jet obtained via Constituent Subtraction method in the presence of the background, we use the matching procedure discussed in Sec. III D to search for its counterpart in the absence of the background, and assign the  $p_T$  of latter as  $p_T^{\text{target}}$ . If its counterpart cannot be found, this jet does not contribute to the residual distribution in Fig. 2. Results here highlight the advantage of the ML methods over the conventional ones on removing the QGP background for predicting the  $p_T$  of quenched jets in relativistic heavy-ion collisions.

For a quantitative comparison between these methods, Tab. I lists the means and standard deviations ( $\sigma$ ) of the residual distributions presented in Figs. 1 and 2 for different estimators evaluated on different testing datasets. This comparison demonstrates the superior performance of the ML model trained on the LBT data to other methods. Although the ML model trained on the combined PYTHIA+LBT data loses certain accuracy compared to that trained solely on the LBT data, the former could be more flexible than the latter in application to diverse environments, e.g., different centralities, of heavy-ion collisions.

## B. Nuclear Modification Factor of Jets

The nuclear modification factor ( $R_{AA}$ ), defined as the ratio of the jet spectrum in A+A collisions, scaled by the

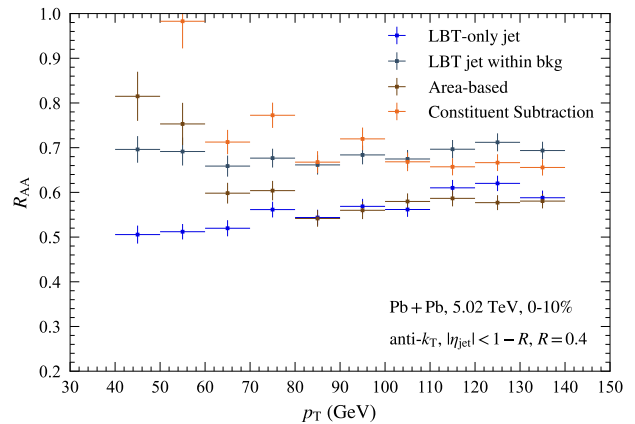


FIG. 4. (Color online) The nuclear modification factor of jets obtained from the Area-based and Constituent Subtraction methods, compared to two baselines of the LBT jets reconstructed with (LBT jet within bkg) or without (LBT-only jet) the background particles.

average number of nucleon-nucleon collisions, to that in  $p + p$  collisions, measures the amount of jet quenching in high-energy heavy-ion collisions. Based on the jet  $p_T$  predicted by various background subtraction methods, we further study the performance of these methods on evaluating the jet  $R_{AA}$ .

In Fig. 3, we compare the jet  $R_{AA}$  between different evaluation methods. The jet spectrum in  $p + p$  collisions is obtained directly from the PYTHIA simulation. For Pb+Pb collisions, we place partons from the LBT simulation into the thermal background, reconstruct jets and then calculate their spectrum based on their  $p_T$  evaluated using different methods, including three ML models trained on the PYTHIA, LBT, and combined PYTHIA+LBT data, respectively. To demonstrate the accuracy of these ML methods, we also add a baseline, named as “LBT jet within background”, which is obtained by directly applying Eq. (4) on the LBT jets reconstructed inside the background. Although all ML models are designed to approximate the results of the LBT jets within the QGP background, the PYTHIA-trained ML model significantly underestimates the  $R_{AA}$ , which primarily stems from its over-subtraction of the background as discussed earlier. The LBT-trained and PYTHIA+LBT-trained ML models provide reasonable matches to the baseline. In Ref. [79], ML models trained separately on PYTHIA and its variants that simulate quenching effects are utilized to extract the jet  $R_{AA}$  with associated uncertainties from the experimental data. Based on our findings, we recommend either excluding PYTHIA jets from separate training datasets or combining them with realistic quenched jets samples to mitigate bias. Training ML models on jet data that capture jet quenching effects is essential for enhancing the reliability of these models in predicting jet observables. We note that our LBT-trained ML model overpredicts the jet  $p_T$  when its target value is below 40 GeV. Considering the

jet spectrum decreases as  $p_T$  increases, this overprediction can lead to an overestimation of the jet  $R_{AA}$  up to  $p_T$  around 60 GeV.

In Fig. 4, we further compare the jet  $R_{AA}$  obtained from the two conventional background subtraction methods to the baseline of the LBT jets reconstructed in the presence of the QGP background (LBT jet within bkg, same as that in Fig. 3). The Area-based method underestimates the jet  $R_{AA}$  at  $p_T > 60$  GeV, largely due to its oversubtraction of the QGP background, as previously discussed in Fig. 2. In contrast, the Constituent Subtraction method provides reasonable  $R_{AA}$  values above 80 GeV, but significantly overpredicts the jet  $R_{AA}$  below 60 GeV. This overprediction at low  $p_T$  can result from the large width of its residual distribution in Fig. 2 combined with the decreasing jet spectrum with the jet  $p_T$ . Comparing between Fig. 3 and Fig. 4, we see the ML models trained using the LBT and PYTHIA+LBT data show better performance than the conventional background subtraction methods in analyzing the jet  $R_{AA}$ .

In fact, “LBT jet within bkg” is not the exact baseline of jets from theoretical calculations. These jets are first reconstructed together with the background particles, and then their  $p_T$  are calculated using only their jet parton components. As discussed in Sec. III D, the presence of a strong medium background can bias the clustering procedure in the first step, and therefore removing the background contribution in the second step cannot guarantee that  $j_{in\ bkg}$  returns to  $j_{real}$ . In Fig. 4, we add another baseline of the LBT jets, which are reconstructed by using jet partons solely from the LBT model output, without being placed inside a medium background. This baseline of  $R_{AA}$ , labeled as “LBT-only jet”, is expected to reflect the medium modification of jets in theoretical calculations. We see an obvious discrepancy between “LBT-only jet” and “LBT jet within bkg”, suggesting that reconstructed jets which are mismatched to their real counterparts, or “fake jets”, severely affect the accuracy of jet observables.

To tackle the challenge from fake jets in estimating the jet  $R_{AA}$ , we apply the matching procedure presented in Sec. III D to pair the LBT jets reconstructed inside the QGP background to those reconstructed without the QGP background. As shown in Fig. 5, the  $R_{AA}$  calculated using the matched jets, labeled as “Matched LBT-only jet”, reproduces the “LBT-only jet” well. The slight underestimation of the  $R_{AA}$  indicates that most LBT-only jets can be paired from reconstructed jets inside the QGP background via this matching procedure, while a few of them fail the matching due to large deflection of their jet axes by including too many soft background particles during jet reconstruction. The  $p_T$  of these matched LBT jets are then used as the target values, instead of Eq. (4), to re-train our ML models. For the first model, we only include reconstructed jets which can be successfully matched to LBT-only jets in the training dataset, while excluding reconstructed jets whose LBT-only counterparts cannot be found. This, labeled as “ML (Matched

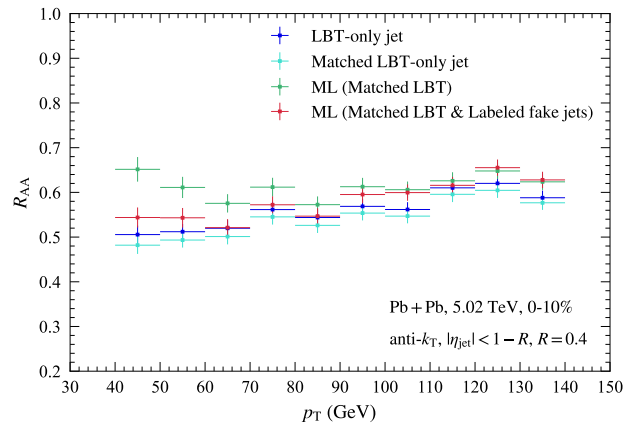


FIG. 5. (Color online) The nuclear modification factor of jets obtained from ML models trained on the matched LBT jet data, with and without labeling the fake jets, compared to the baseline of the LBT jets reconstructed without the background (LBT-only jet) and a direct calculation using the matched LBT jets (Matched LBT-only jet).

LBT)”, significantly narrows the difference between our model output and the LBT-only jet baseline compared to earlier results in Figs. 3 and 4. Noticeable difference still remains at  $p_T < 80$  GeV because this ML model does not recognize fake jets and would still predict  $p_T$  values for them. For the second model, besides labeling the  $p_T$  of reconstructed jets inside the background as the  $p_T$  of their matched LBT-only jets, as we did for the first model, we label the  $p_T$  of fake jets as zero during the model training. This model, labeled as “Matched LBT & Labeled fake jets”, further improves the  $R_{AA}$  prediction, which aligns closely with the baseline of the LBT-only jets down to  $p_T$  around 40 GeV. Results in Fig. 5 reveal the importance of properly dealing with fake jets in training ML models for their accurate predictions on jet observables. Although conventional methods, e.g., the Mixed-Events method [109], have also been developed for subtracting contributions from fake jets, these methods are usually implemented on an event averaged basis, not as flexible as the ML methods which can be implemented on a jet-by-jet basis and conveniently extended to more complicated jet observables like jet substructures.

## V. CONCLUSIONS

We have applied the machine learning techniques on reconstructing jet momentum within the QGP background in relativistic heavy-ion collisions. By training the DNN models on simulated data from both PYTHIA and LBT models for comparative analysis, we have demonstrated that the ML-based reconstruction, when properly taking into account the jet quenching effects, achieves high accuracy in jet momentum reconstruction within the QGP background. In particular, while the model trained on the PYTHIA data accurately predicts the  $p_T$  of vacuum

(PYTHIA) jets, it exhibits significant bias when being applied to medium-modified (LBT) jets, primarily due to an oversubtraction of the medium response particles from jet-medium interactions, which resemble the background particles but belong to jets. However, by training on the quenched jet data generated by the LBT model, the DNN model effectively reduces this prediction bias and performs a more accurate background subtraction compared to the conventional Area-based and Constituent Subtraction methods. The DNN model trained on a combined PYTHIA+LBT dataset appears equally effective, and is generalizable to more diverse environments.

This improvement is also highlighted in our analyses of the nuclear modification factor of jets, where the LBT-trained model and the PYTHIA+LBT-trained model excel in approximating the baseline of the reconstructed LBT jets within the QGP background, compared to the conventional methods, across a wide  $p_T$  range. In order to further accurately reproduce the baseline of the jet quenching effects, we introduce a matching procedure to pair jets inside the QGP background to their counterparts reconstructed in the absence of the background. This eliminates the contamination from fake jets and allows an accurate extraction of the jet quenching effects from the experimental data. Our ML models trained on the  $p_T$  of the matched-LBT jets, especially when fake jets are explicitly labeled, provide successful predictions of the theoretical baseline of the jet  $R_{AA}$ .

This work demonstrates that machine learning pro-

vides a powerful approach for jet momentum reconstruction within a complicated QGP background, extending a reliable jet momentum reconstruction down to  $p_T$  around 40 GeV, which can be hardly achieved by conventional methods. Our results underscore the importance of training models on quenching-aware datasets to ensure accurate background subtraction in relativistic heavy-ion collisions, as well as the importance of identifying fake jets in training ML models to achieve reliable predictions on jet observables. Future efforts could focus on reducing model bias by training on data from diverse jet quenching models and realistic heavy-ion backgrounds with collective flows. This expanded approach could further enhance the applicability of ML techniques in reconstructing other jet observables, enabling a deeper understanding of the QGP properties and advancing the field of high-energy nuclear physics.

## ACKNOWLEDGMENTS

We are grateful to helpful discussions with Yang He, Maowu Nie and Long-Gang Pang. This work is supported in part by the National Natural Science Foundation of China (NSFC) under Grant Nos. 12175122, 2021-867 (R.L., S.C.), and in part by the Taishan Scholars Program under Grant No. tsqzn20221162, and Shandong Excellent Young Scientists Fund Program (Overseas) under Grant No. 2023HWYQ-106 (Y.D.).

- 
- [1] M. Gyulassy and L. McLerran, *Nucl. Phys. A* **750**, 30 (2005), [arXiv:nucl-th/0405013](#).
  - [2] P. Jacobs and X.-N. Wang, *Prog. Part. Nucl. Phys.* **54**, 443 (2005), [arXiv:hep-ph/0405125](#).
  - [3] W. Busza, K. Rajagopal, and W. van der Schee, *Ann. Rev. Nucl. Part. Sci.* **68**, 339 (2018), [arXiv:1802.04801 \[hep-ph\]](#).
  - [4] H. Elfner and B. Müller, *J. Phys. G* **50**, 103001 (2023), [arXiv:2210.12056 \[nucl-th\]](#).
  - [5] X.-N. Wang and M. Gyulassy, *Phys. Rev. Lett.* **68**, 1480 (1992).
  - [6] K. M. Burke *et al.* (JET), *Phys. Rev. C* **90**, 014909 (2014), [arXiv:1312.5003 \[nucl-th\]](#).
  - [7] S. Cao *et al.* (JETSCAPE), *Phys. Rev. C* **104**, 024905 (2021), [arXiv:2102.11337 \[nucl-th\]](#).
  - [8] M. Xie, W. Ke, H. Zhang, and X.-N. Wang, *Phys. Rev. C* **108**, L011901 (2023), [arXiv:2206.01340 \[hep-ph\]](#).
  - [9] B. Chen, X. Chen, X. Li, Z.-R. Zhu, and K. Zhou, (2024), [arXiv:2404.18217 \[hep-ph\]](#).
  - [10] S. A. Bass, C. Gale, A. Majumder, C. Nonaka, G.-Y. Qin, T. Renk, and J. Ruppert, *Phys. Rev. C* **79**, 024901 (2009), [arXiv:0808.0908 \[nucl-th\]](#).
  - [11] G.-Y. Qin and X.-N. Wang, *Int. J. Mod. Phys. E* **24**, 1530014 (2015), [arXiv:1511.00790 \[hep-ph\]](#).
  - [12] A. Majumder and M. Van Leeuwen, *Prog. Part. Nucl. Phys.* **66**, 41 (2011), [arXiv:1002.2206 \[hep-ph\]](#).
  - [13] J.-P. Blaizot and Y. Mehtar-Tani, *Int. J. Mod. Phys. E* **24**, 1530012 (2015), [arXiv:1503.05958 \[hep-ph\]](#).
  - [14] Y. Mehtar-Tani, J. G. Milhano, and K. Tywoniuk, *Int. J. Mod. Phys. A* **28**, 1340013 (2013), [arXiv:1302.2579 \[hep-ph\]](#).
  - [15] S. Cao and X.-N. Wang, *Rept. Prog. Phys.* **84**, 024301 (2021), [arXiv:2002.04028 \[hep-ph\]](#).
  - [16] S. Cao and G.-Y. Qin, *Ann. Rev. Nucl. Part. Sci.* **73**, 205 (2023), [arXiv:2211.16821 \[nucl-th\]](#).
  - [17] S. Cao, A. Majumder, R. Modarresi-Yazdi, I. Soudi, and Y. Tachibana, *Int. J. Mod. Phys. E* **33**, 2430002 (2024), [arXiv:2401.10026 \[hep-ph\]](#).
  - [18] B. Schenke, C. Gale, and S. Jeon, *Phys. Rev. C* **80**, 054913 (2009), [arXiv:0909.2037 \[hep-ph\]](#).
  - [19] K. C. Zapp, *Eur. Phys. J. C* **74**, 2762 (2014), [arXiv:1311.0048 \[hep-ph\]](#).
  - [20] J. Casalderrey-Solana, D. C. Gulhan, J. G. Milhano, D. Pablos, and K. Rajagopal, *JHEP* **10**, 019 (2014), [Erratum: *JHEP* 09, 175 (2015)], [arXiv:1405.3864 \[hep-ph\]](#).
  - [21] S. Cao and A. Majumder, *Phys. Rev. C* **101**, 024903 (2020), [arXiv:1712.10055 \[nucl-th\]](#).
  - [22] S. Cao *et al.* (JETSCAPE), *Phys. Rev. C* **96**, 024909 (2017), [arXiv:1705.00050 \[nucl-th\]](#).
  - [23] J. H. Putschke *et al.*, (2019), [arXiv:1903.07706 \[nucl-th\]](#).
  - [24] T. Luo, Y. He, S. Cao, and X.-N. Wang, *Phys. Rev. C* **109**, 034919 (2024), [arXiv:2306.13742 \[nucl-th\]](#).
  - [25] I. Karpenko, A. Lind, M. Rohrmoser, J. Aichelin, and P.-B. Gossiaux, (2024), [arXiv:2404.14579 \[hep-ph\]](#).



- [26] L. Apolinário, Y.-T. Chien, and L. Cunqueiro Mendez, *Int. J. Mod. Phys. E* **33**, 2430003 (2024).
- [27] J. Casalderrey-Solana, D. Gulhan, G. Milhano, D. Pablos, and K. Rajagopal, *JHEP* **03**, 135 (2017), [arXiv:1609.05842 \[hep-ph\]](#).
- [28] Y. Tachibana, N.-B. Chang, and G.-Y. Qin, *Phys. Rev. C* **95**, 044909 (2017), [arXiv:1701.07951 \[nucl-th\]](#).
- [29] R. Kunnawalkam Elayavalli and K. C. Zapp, *JHEP* **07**, 141 (2017), [arXiv:1707.01539 \[hep-ph\]](#).
- [30] G. Milhano, U. A. Wiedemann, and K. C. Zapp, *Phys. Lett. B* **779**, 409 (2018), [arXiv:1707.04142 \[hep-ph\]](#).
- [31] W. Chen, S. Cao, T. Luo, L.-G. Pang, and X.-N. Wang, *Phys. Lett. B* **810**, 135783 (2020), [arXiv:2005.09678 \[hep-ph\]](#).
- [32] C. Park, S. Jeon, and C. Gale, *Nucl. Phys. A* **982**, 643 (2019), [arXiv:1807.06550 \[nucl-th\]](#).
- [33] T. Luo, S. Cao, Y. He, and X.-N. Wang, *Phys. Lett. B* **782**, 707 (2018), [arXiv:1803.06785 \[hep-ph\]](#).
- [34] J. Casalderrey-Solana, G. Milhano, D. Pablos, and K. Rajagopal, *JHEP* **01**, 044 (2020), [arXiv:1907.11248 \[hep-ph\]](#).
- [35] N.-B. Chang, Y. Tachibana, and G.-Y. Qin, *Phys. Lett. B* **801**, 135181 (2020), [arXiv:1906.09562 \[nucl-th\]](#).
- [36] Y. Tachibana, C. Shen, and A. Majumder, *Phys. Rev. C* **106**, L021902 (2022), [arXiv:2001.08321 \[nucl-th\]](#).
- [37] Z. Yang, Y. He, I. Moulton, and X.-N. Wang, *Phys. Rev. Lett.* **132**, 011901 (2024), [arXiv:2310.01500 \[hep-ph\]](#).
- [38] W.-J. Xing, S. Cao, G.-Y. Qin, and X.-N. Wang, (2024), [arXiv:2409.12843 \[hep-ph\]](#).
- [39] F.-L. Liu, X.-Y. Wu, S. Cao, G.-Y. Qin, and X.-N. Wang, *Phys. Lett. B* **848**, 138355 (2024), [arXiv:2304.08787 \[hep-ph\]](#).
- [40] B. Karmakar, D. Zigic, I. Salom, J. Auvinen, P. Huovinen, M. Djordjevic, and M. Djordjevic, *Phys. Rev. C* **108**, 044907 (2023), [arXiv:2305.11318 \[hep-ph\]](#).
- [41] B. Karmakar, D. Zigic, M. Djordjevic, P. Huovinen, M. Djordjevic, and J. Auvinen, *Phys. Rev. C* **110**, 044906 (2024), [arXiv:2403.17817 \[hep-ph\]](#).
- [42] M. Cacciari, G. P. Salam, and G. Soyez, *Eur. Phys. J. C* **72**, 1896 (2012), [arXiv:1111.6097 \[hep-ph\]](#).
- [43] B. Abelev *et al.* (ALICE), *JHEP* **03**, 013 (2014), [arXiv:1311.0633 \[nucl-ex\]](#).
- [44] P. Berta, L. Masetti, D. W. Miller, and M. Spousta, *JHEP* **08**, 175 (2019), [arXiv:1905.03470 \[hep-ph\]](#).
- [45] “JetToyHI: framework to study jet substructure in heavy ion environment,” <https://github.com/mverwe/JetToyHI>.
- [46] S. Pratt, E. Sangaline, P. Sorensen, and H. Wang, *Phys. Rev. Lett.* **114**, 202301 (2015).
- [47] J. E. Bernhard, J. S. Moreland, S. A. Bass, J. Liu, and U. Heinz, *Phys. Rev. C* **94**, 024907 (2016).
- [48] J. E. Bernhard, J. S. Moreland, and S. A. Bass, *Nature Phys.* **15**, 1113 (2019).
- [49] J. S. Moreland, J. E. Bernhard, and S. A. Bass, *Phys. Rev. C* **101**, 024911 (2020).
- [50] G. Nijs, W. van der Schee, U. Gürsoy, and R. Snellings, *Phys. Rev. Lett.* **126**, 202301 (2021).
- [51] G. Nijs, W. van der Schee, U. Gürsoy, and R. Snellings, *Phys. Rev. C* **103**, 054909 (2021).
- [52] Y. Xu, J. E. Bernhard, S. A. Bass, M. Nahrgang, and S. Cao, *Phys. Rev. C* **97**, 014907 (2018).
- [53] R. S. Bhalerao, J.-Y. Ollitrault, S. Pal, and D. Teaney, *Phys. Rev. Lett.* **114**, 152301 (2015), [arXiv:1410.7739 \[nucl-th\]](#).
- [54] A. Mazeliauskas and D. Teaney, *Phys. Rev. C* **91**, 044902 (2015), [arXiv:1501.03138 \[nucl-th\]](#).
- [55] L.-G. Pang, K. Zhou, N. Su, H. Petersen, H. Stöcker, and X.-N. Wang, *Nature Commun.* **9**, 210 (2018), [arXiv:1612.04262 \[hep-ph\]](#).
- [56] Z. Liu, W. Zhao, and H. Song, *Eur. Phys. J. C* **79**, 870 (2019), [arXiv:1903.09833 \[nucl-th\]](#).
- [57] Y.-L. Du, K. Zhou, J. Steinheimer, L.-G. Pang, A. Motornenko, H.-S. Zong, X.-N. Wang, and H. Stöcker, *Eur. Phys. J. C* **80**, 516 (2020), [arXiv:1910.11530 \[hep-ph\]](#).
- [58] J. He, W.-B. He, Y.-G. Ma, and S. Zhang, *Phys. Rev. C* **104**, 044902 (2021).
- [59] N. Mallick, S. Tripathy, A. N. Mishra, S. Deb, and R. Sahoo, *Phys. Rev. D* **103**, 094031 (2021), [arXiv:2103.01736 \[hep-ph\]](#).
- [60] Y. Wang, F. Li, Q. Li, H. Lü, and K. Zhou, *Phys. Lett. B* **822**, 136669 (2021), [arXiv:2107.11012 \[nucl-th\]](#).
- [61] A. Boehnlein, M. Diefenthaler, N. Sato, M. Schram, V. Ziegler, C. Fanelli, M. Hjorth-Jensen, T. Horn, M. P. Kuchera, D. Lee, W. Nazarewicz, P. Ostroumov, K. Orginos, A. Poon, X.-N. Wang, A. Scheinker, M. S. Smith, and L.-G. Pang, *Rev. Mod. Phys.* **94**, 031003 (2022).
- [62] P. Xiang, Y.-S. Zhao, and X.-G. Huang, *Chin. Phys. C* **46**, 074110 (2022), [arXiv:2112.03824 \[hep-ph\]](#).
- [63] S. Shi, K. Zhou, J. Zhao, S. Mukherjee, and P. Zhuang, *Phys. Rev. D* **105**, 014017 (2022), [arXiv:2105.07862 \[hep-ph\]](#).
- [64] F.-P. Li, H.-L. Lü, L.-G. Pang, and G.-Y. Qin, *Phys. Lett. B* **844**, 138088 (2023), [arXiv:2211.07994 \[hep-ph\]](#).
- [65] O. Soloveva, A. Palermo, and E. Bratkovskaya, *Phys. Rev. C* **110**, 034908 (2024), [arXiv:2311.15984 \[hep-ph\]](#).
- [66] K. Zhou, L. Wang, L.-G. Pang, and S. Shi, *Prog. Part. Nucl. Phys.* **135**, 104084 (2024), [arXiv:2303.15136 \[hep-ph\]](#).
- [67] Y. Du, *PoS HardProbes2023*, 030 (2024).
- [68] Y.-L. Du, D. Pablos, and K. Tywoniuk, *PoS PANIC2021*, 224 (2022), [arXiv:2112.00681](#).
- [69] Y.-T. Chien and R. Kunnawalkam Elayavalli, (2018), [arXiv:1803.03589 \[hep-ph\]](#).
- [70] L. Apolinário, N. F. Castro, M. Crispim Romão, J. G. Milhano, R. Pedro, and F. C. R. Peres, *JHEP* **11**, 219 (2021), [arXiv:2106.08869 \[hep-ph\]](#).
- [71] L. Liu, J. Velkovska, Y. Wu, and M. Verweij, *JHEP* **04**, 140 (2023), [arXiv:2206.01628 \[hep-ph\]](#).
- [72] Y. S. Lai, J. Mulligan, M. Płoskoń, and F. Ringer, *JHEP* **10**, 011 (2022), [arXiv:2111.14589 \[hep-ph\]](#).
- [73] M. Crispim Romão, J. G. Milhano, and M. van Leeuwen, *SciPost Phys.* **16**, 015 (2024), [arXiv:2304.07196 \[hep-ph\]](#).
- [74] U. S. Qureshi and R. K. Elayavalli, [arXiv:2411.19389 \(2024\)](#).
- [75] Y.-L. Du, D. Pablos, and K. Tywoniuk, *JHEP* **21**, 206 (2020), [arXiv:2012.07797 \[hep-ph\]](#).
- [76] Y.-L. Du, D. Pablos, and K. Tywoniuk, *Phys. Rev. Lett.* **128**, 012301 (2022).
- [77] Z. Yang, Y. He, W. Chen, W.-Y. Ke, L.-G. Pang, and X.-N. Wang, *Eur. Phys. J. C* **83**, 652 (2023), [arXiv:2206.02393 \[nucl-th\]](#).
- [78] R. Haake and C. Loizides, *Phys. Rev. C* **99**, 064904 (2019), [arXiv:1810.06324 \[nucl-ex\]](#).
- [79] S. Acharya *et al.* (ALICE), *Phys. Lett. B* **849**, 138412 (2024), [arXiv:2303.00592 \[nucl-ex\]](#).

- [80] T. Mengel, P. Steffanic, C. Hughes, A. C. O. da Silva, and C. Nattrass, *Phys. Rev. C* **108**, L021901 (2023), [arXiv:2303.08275 \[hep-ex\]](#).
- [81] T. Sjöstrand, S. Mrenna, and P. Z. Skands, *JHEP* **05**, 026 (2006), [arXiv:hep-ph/0603175](#).
- [82] T. Sjöstrand, S. Ask, J. R. Christiansen, R. Corke, N. Desai, P. Ilten, S. Mrenna, S. Prestel, C. O. Rasmussen, and P. Z. Skands, *Comput. Phys. Commun.* **191**, 159 (2015), [arXiv:1410.3012 \[hep-ph\]](#).
- [83] M. Cacciari, G. P. Salam, and G. Soyez, *JHEP* **04**, 063 (2008), [arXiv:0802.1189 \[hep-ph\]](#).
- [84] Y. L. Dokshitzer, G. Leder, S. Moretti, and B. Webber, *JHEP* **08**, 001 (1997), [arXiv:hep-ph/9707323](#).
- [85] M. Wobisch and T. Wengler, in *Workshop on Monte Carlo Generators for HERA Physics (Plenary Starting Meeting)* (1998) pp. 270–279, [arXiv:hep-ph/9907280](#).
- [86] S. Cao, T. Luo, G.-Y. Qin, and X.-N. Wang, *Phys. Rev. C* **94**, 014909 (2016), [arXiv:1605.06447 \[nucl-th\]](#).
- [87] Y. He, T. Luo, X.-N. Wang, and Y. Zhu, *Phys. Rev. C* **91**, 054908 (2015), [Erratum: *Phys. Rev. C* **97**, 019902 (2018)], [arXiv:1503.03313 \[nucl-th\]](#).
- [88] X.-F. Guo and X.-N. Wang, *Phys. Rev. Lett.* **85**, 3591 (2000), [arXiv:hep-ph/0005044 \[hep-ph\]](#).
- [89] X.-N. Wang and X.-F. Guo, *Nucl. Phys.* **A696**, 788 (2001), [arXiv:hep-ph/0102230 \[hep-ph\]](#).
- [90] B.-W. Zhang and X.-N. Wang, *Nucl. Phys.* **A720**, 429 (2003), [arXiv:hep-ph/0301195 \[hep-ph\]](#).
- [91] A. Majumder, *Phys. Rev. D* **85**, 014023 (2012), [arXiv:0912.2987 \[nucl-th\]](#).
- [92] B.-W. Zhang, E. Wang, and X.-N. Wang, *Phys. Rev. Lett.* **93**, 072301 (2004), [arXiv:nucl-th/0309040 \[nucl-th\]](#).
- [93] B.-W. Zhang, E.-K. Wang, and X.-N. Wang, *Nucl. Phys.* **A757**, 493 (2005), [arXiv:hep-ph/0412060 \[hep-ph\]](#).
- [94] Y.-L. Du, Y. He, X.-N. Wang, H. Xing, and H.-S. Zong, *Phys. Rev. D* **98**, 054015 (2018).
- [95] Y.-Y. Zhang, G.-Y. Qin, and X.-N. Wang, *Phys. Rev. D* **100**, 074031 (2019), [arXiv:1905.12699 \[hep-ph\]](#).
- [96] C. Sirimanna, S. Cao, and A. Majumder, *Phys. Rev. C* **105**, 024908 (2022), [arXiv:2108.05329 \[hep-ph\]](#).
- [97] L.-G. Pang, H. Petersen, and X.-N. Wang, *Phys. Rev. C* **97**, 064918 (2018), [arXiv:1802.04449 \[nucl-th\]](#).
- [98] X.-Y. Wu, G.-Y. Qin, L.-G. Pang, and X.-N. Wang, *Phys. Rev. C* **105**, 034909 (2022), [arXiv:2107.04949 \[hep-ph\]](#).
- [99] W.-J. Xing, S. Cao, G.-Y. Qin, and H. Xing, *Phys. Lett. B* **805**, 135424 (2020), [arXiv:1906.00413 \[hep-ph\]](#).
- [100] Y. He, S. Cao, W. Chen, T. Luo, L.-G. Pang, and X.-N. Wang, *Phys. Rev. C* **99**, 054911 (2019), [arXiv:1809.02525 \[nucl-th\]](#).
- [101] Y. He, W. Chen, T. Luo, S. Cao, L.-G. Pang, and X.-N. Wang, *Phys. Rev. C* **106**, 044904 (2022), [arXiv:2201.08408 \[hep-ph\]](#).
- [102] S. Acharya *et al.* (ALICE), *Phys. Rev. C* **101**, 044907 (2020), [arXiv:1910.07678 \[nucl-ex\]](#).
- [103] P. Skands, S. Carrazza, and J. Rojo, *Eur. Phys. J. C* **74**, 3024 (2014), [arXiv:1404.5630 \[hep-ph\]](#).
- [104] M. Zhang, Y. He, S. Cao, and L. Yi, *Chin. Phys. C* **47**, 024106 (2023), [arXiv:2208.13331 \[nucl-th\]](#).
- [105] S. Catani, Y. L. Dokshitzer, M. H. Seymour, and B. R. Webber, *Nucl. Phys. B* **406**, 187 (1993).
- [106] S. D. Ellis and D. E. Soper, *Phys. Rev. D* **48**, 3160 (1993), [arXiv:hep-ph/9305266](#).
- [107] M. Cacciari, G. P. Salam, and G. Soyez, *JHEP* **04**, 005 (2008), [arXiv:0802.1188 \[hep-ph\]](#).
- [108] D. P. Kingma and J. Ba, [arXiv:1412.6980](#) (2014).
- [109] L. Adamczyk *et al.* (STAR), *Phys. Rev. C* **96**, 024905 (2017), [arXiv:1702.01108 \[nucl-ex\]](#).